REGULAR PAPER

The aerodynamic force estimation of a swept-wing UAV using ANFIS based on metaheuristic algorithms

M. Uzun[1], H.H. Bilgic[2] (ID), E.H. Çopur[3] (ID) and S. Çoban[1] (ID)

[1]Department of Airframe and Powerplant Maintenance, İskenderun Technical University, İskenderun, Türkiye, [2]Department of Aeronautical Engineering, Necmettin Erbakan University, Konya, Türkiye and [3]Department of Astronautical Engineering, Necmettin Erbakan University, Konya, Türkiye
Corresponding author: H. H. Bilgic; Email: hhbilgic@erbakan.edu.tr

Abstract

In this paper, a new approach to modeling and controlling the problems associated with a morphing unmanned aerial vehicle (UAV) is proposed. Within the scope of the study, a dataset was created by obtaining a wide range of aerodynamic parameters for the UAV with Ansys Fluent under variable conditions using the computational fluid dynamics approach. For this, a large dataset was created that considered 5 different angles of attack, 14 different swept angles, and 5 different velocities. While creating the dataset, the analyses were verified by considering studies that have been experimentally validated in the literature. Then, an artificial intelligence-based model was created using the dataset obtained. Metaheuristic algorithms such as the artificial bee colony algorithm, ant colony algorithm and genetic algorithms are used to increase the modeling success of the adaptive neuro-fuzzy inference system (ANFIS) approach. A novel modeling approach is proposed that constitutes a new decision support system for real-time flight. According to the results obtained, all the ANFIS models based on metaheuristic algorithms were more successful than the traditional approach, the multilinear regression model. The swept angle that meets the minimum lift needed by the UAV for different flight conditions was estimated with the help of the designed decision support system. Thus, the drag force is minimised while obtaining the required lift force. The performance of the UAV was compared with the nonmorphing configuration, and the results are presented in tables and graphs.

Nomenclature

Definitions/Abbreviations

UAV	unmanned aerial vehicle
ANFIS	adaptive neuro-fuzzy inference system
CFD	computational fluid dynamics
PSO	particle swarm optimisation
ACO	ant colony optimisation
GA	genetic algorithm
m	UAV mass
pitch	propeller pitch
S	wing area
rpm	propeller revolution per minute
$\wedge$	wing swept angle
λ	taper ratio of wing
U_0	UAV velocity
Q	dynamic pressure
C_{L0}	aircraft reference lift coefficient
AR	wing aspect ratio

b	span
$\bar{c}$	wing mean aerodynamic chord
C_{D0}	UAV reference drag coefficient
P_{req}	power require
T_{req}	thrust require
D	drag force
L	lift force
V	velocity
C_L	lift coefficient
C_D	drag coefficient
W	UAV weight
ρ	air density
e	Oswald number

1.0 Introduction

The flight performance of UAVs can be determined via certain key design metrics, namely maximum endurance, maximum ceiling height, path-following capability and range. These metrics can be improved by enhanced flight control algorithms, the dimension optimisation of the geometric parameters and the implementation of an effective battery management system. In the literature, different methods such as variable geometry structures, adaptive controllers and hybrid battery management systems have been reported to improve UAV flight performance [1–3].

Swept wing geometry is one of the effective configurations to improve the flight performance of UAVs. The swept angle is defined as the angle between the leading edge of the wing and the lateral axis of the aircraft. The swept angle has considerable influence on various parameters such as lift curve slope, maximum lift coefficient and induced drag coefficient. It also reduces the drag force, allowing aircraft to cruise at higher velocities. Subsonic aircraft with swept wings are capable of reaching higher Mach numbers with the help of drag divergence. This means that the swept angle of the subsonic aircraft wing causes drag divergence to occur at higher Mach numbers [4].

The morphing swept wing concept was recently applied to benefit from the aforementioned advantages of the swept angle in different flight conditions [5–7]. In the literature, it is stated that this new design offers several advantages: improved take-off and landing performance, reduced drag force, good flight characteristics and increased efficiency due to an optimum lift/drag ratio during flight. However, it also suffers from certain disadvantages, which include the complexity and cost of the connection mechanism, the additional weight of the control systems and the aerodynamic centre shift due to the change in the swept angle. In morphing swept wing aircraft, the aim is to increase efficiency by using a low swept angle at low velocities and high swept angle at high velocities [8].

Yan et al. performed simulations on an aircraft model with variable swept angles. In this study, an adaptive sliding mode controller (SMC) was designed to overcome the difficulties in mathematical modeling that would otherwise arise due to the morphing mechanism. The controller performance was examined in comparison with a traditional SMC [9]. Xu et al. applied a switching controller designed on a nonlinear aircraft model with variable swept angles that also considered actuator dynamics. The stability of the control system was investigated using the Lyapunov stability theory, and its performance was demonstrated in simulations [10]. Dai et al. designed four different wing configurations for an aircraft and examined their performance under subsonic, supersonic and hypersonic flight conditions. In their comparative study, their results revealed that better aerodynamic performance and a wider flight velocity range can be achieved by selecting the appropriate wing configuration for different flight conditions [11]. Roy and Peyada applied the ABC algorithm-based ANFIS approach to noisy data recorded during flight to estimate the aerodynamic parameters, further pointing out that their method can be used as a decision support system to improve the stability of the aircraft [12]. However, in these previous studies, a model that can predict the changes in the lift and drag forces of the aircraft under variable flight conditions (variable velocity) and geometry (variable swept angle) has not been obtained.
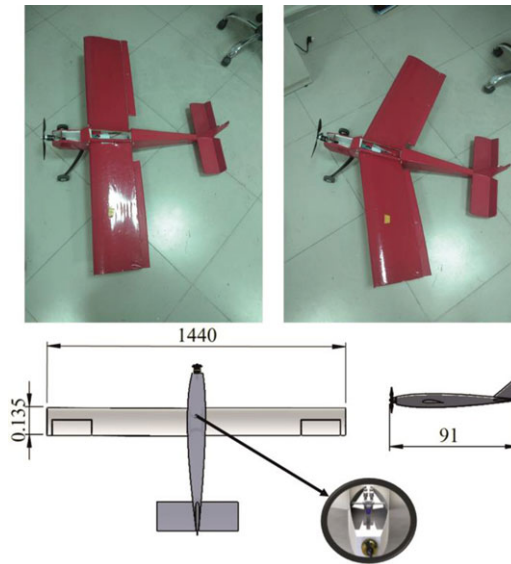
Figure 1. *The concept design of swept wing UAV.*

In this study, a unique aircraft configuration with adjustable swept angle is designed and Clark-Y, which is one of the most widely used aerofoil types, is taken to be the wing aerofoil. The first aim of the study was to estimate the swept angle that would achieve the minimum lift force under different flight conditions. Thus, it is aimed to gain from the drag force.

The second aim is to increase the range of the aircraft with low drag force at high velocities. In addition, the runway distance required for take-off can be shortened with zero swept angle, namely in a straight-wing configuration. To achieve the desired performance, it is necessary to make predictions about the behaviour of the aircraft under different flight conditions. For this reason, the aerodynamic performance of the swept wing aircraft designed in this study is evaluated at 5 different velocities along with 5 different angles of attack and 14 different swept angles. For each case, the drag fore and lift force are computed using computational fluid dynamics methods. The numerical results are validated through comparison with experimental data in the literature [13, 14]. Thus, a large, validated numerical dataset will be generated. Then, three artificial intelligence models based on metaheuristic algorithms are developed by using the obtained data. To demonstrate the effectiveness of the artificial intelligence models, the model performances are assessed and validated using the traditional multilinear regression model. According to the statistical measures used in the comparative results, the genetic algorithm-based model produces a lower estimation error than the other models, and was therefore selected to estimate the lift and drag forces. To estimate the swept angle required to maintain the minimum lifting force and reduce the drag force in different flight conditions, a decision support system has been developed for the selected artificial intelligence model. The flight performance obtained using the decision support system was compared with the nonmorphing UAV configuration in the simulation environment.

2.0 Theoretical background for cfd and optimisation methods

In this section, the design criteria for a UAV with a variable swept angle are briefly described. In Fig. 1, the dimensions of the designed UAV are given, and the morphing mechanism used to change the swept angle of the wing is schematically illustrated. The morphing mechanism consists of one servo motor and two gears placed on the leading edge of each wing. In addition, the wing is supported by bearings mounted on the fuselage, and the morphing is constrained on the horizontal plane.

Table 1. *Technical specification of the swept wing UAV*

Feature	Size	Feature	Size
Weight	2,213 gr	Propeller diameter	11in
Wingspan	1,440 cm	Propeller pitch	5.5 in
Body length	91 cm	Propeller RPM	14,040/min
Wing area	0.203852 m²	Horizontal tail area	0.073477 m²
Wing mean aerodynamic chord	0.135 m		
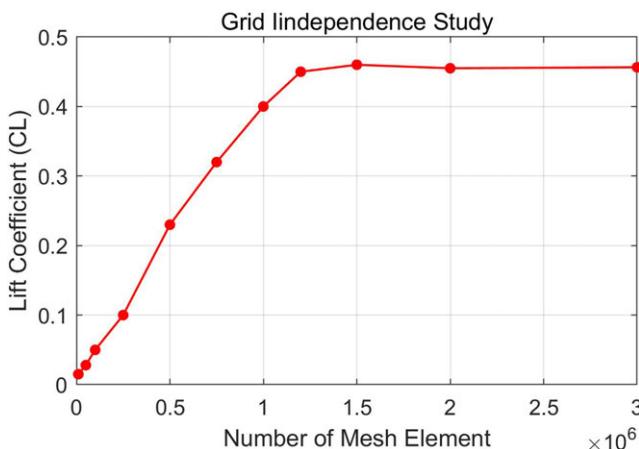
Figure 2. *The effect of mesh element number on the lift coefficient.*

The technical specifications of the designed swept UAV are presented in Table 1.

2.1 Numerical method

2.1.1 The grid independence study

Grid independence is a very important parameter, especially in the numerical analysis of computational fluid dynamics (CFD) applications. The network structure parameters, namely the number of cells, or the number of nodes in the analysis, greatly affect the accuracy of the solution. An increased number of nodes or number of cells used lead to more accurate results but at the expense of increased usage of computational resources in the analysis. For this reason, studies should be independent of the network structure. A grid independence study was carried out to determine the optimum mesh number. With the grid independence study, the optimum number of meshes can be solved in the shortest time [15].

Since time and central processing unit (CPU) power are significant parameters in the analysis process, an optimisation should be performed to find the balance between the accuracy of, and the computational cost of finding, the solution. Therefore, the optimum mesh element number is determined and given in Fig. 2.

2.1.2 Boundary conditions

While determining the flow area, a distance of $15\bar{c}$ above and below the nose of the aircraft was determined to be the limit. On the trailing edges, a distance of $20\bar{c}$ to the outward was determined as the limit. No-slip boundary conditions have been used on solid surfaces. Figure 3 presents the flow field boundary conditions.

Table 2. *Mesh properties and skewness and orthogonal quality mesh metrics spectra*

Minimum element size	0.00005m	Skewness (max)	0.72599
Number of elements	8,015,264	Growth rate	1.12
Maximum size	0.1 m	Curvature normal angle	18°
Orthogonal quality	0.2702	Mesh method	Patch conforming/sweeping
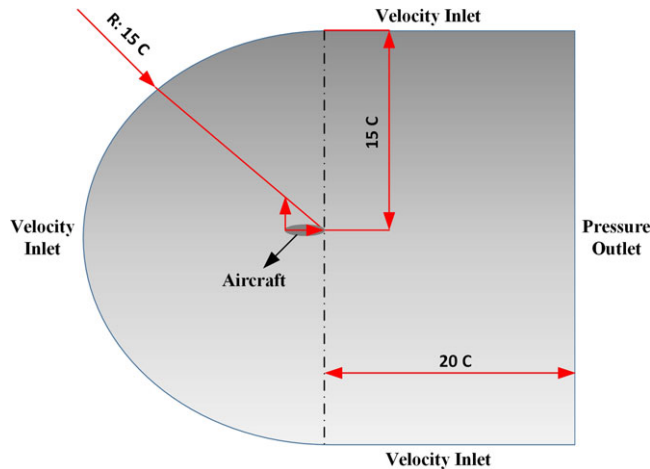
Figure 3. *The dimensions and boundary conditions of the computational domain.*
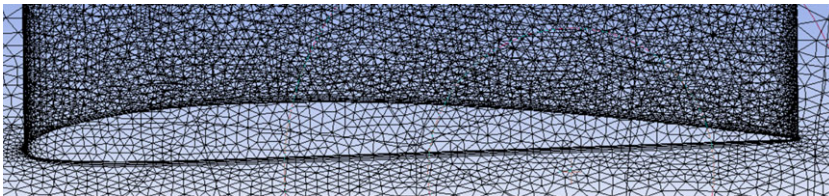
Figure 4. *Mesh inflation image.*

2.1.3 Mesh properties

As seen in Fig. 4, the mesh structure created in the calculation area is intense in the regions close to the aerofoil, while being less intense in regions that are more distal. The mesh number is optimised using the 1.2 growing mesh size from the wing surface to the outer flow region. The reason for the application of such a network structure is to take up less space on the computer on which the numerical analysis is performed, and to aim to conduct the analyses in a shorter time. To monitor the flow events (flow separation bubble, reverse flow, reattachment, turbulent flow, etc.) on the wing surface more clearly, a boundary layer was created with the inflection parameter. Mesh properties and skewness and orthogonal quality mesh metrics spectra are given in Table 2.

2.2 Computing approaches

The k-ω SST turbulence model blends the formulation of the Wilcox k-ω model [16] in the near-wall region with the formulation of the k-ϵ model [17] in the far-field developed by Menter [18]. This model also includes the modeling of the SST using the modified definition of turbulent viscosity. The k-ω SST transition model solves four transport equations k, specific turbulence dissipation rate (ω), intermittency

(γ) and transition onset momentum thickness Reynolds number (Reθt) equations. The use of a k-ω formulation in the inner parts of the boundary layer makes the model directly usable all the way down to the wall through the viscous sublayer; hence, the SST k-ω model can be used as a low-re turbulence model without the need for any extra damping functions. The SST formulation also switches to a k-ϵ behaviour in the free-stream and thereby avoids the common k-ω problem that the model is too sensitive to the inlet free-stream turbulence properties. Authors who use the SST k-ω model often credit it for its good behaviour in adverse pressure gradients and separating flow. The SST k-ω model does produce relatively large turbulence levels in regions with large normal strain, such as stagnation regions and regions with strong acceleration. This tendency is much less pronounced than that with a normal k-ϵ model, though.

2.3 Turbulence models used in aircraft analysis

2.3.1 SST k-ω turbulence model

The shear stress transport (SST) k-ω turbulence model, which is accepted as the turbulence model that gives the best results in external flow aerodynamic applications or in simulations where flow separations are important, is used together with k-ω and k-ϵ. Among these models, the k-ω model gives better results in regions close to the wall, but it is inadequate in free-flow regions that are more distal. On the other hand, the k-ϵ turbulence model gives good results in free-flow regions.

$$\frac{\partial(\rho\omega)}{\partial t} + \nabla(\rho V\omega) = \nabla\left(\left(\mu + \frac{\mu_t}{\sigma_\omega}\right)\nabla_\omega\right) + \frac{\gamma}{v_t}P_k - \beta\rho\omega^2 + \underbrace{2(1-F_1)\frac{\rho\sigma\omega_2}{\omega}\nabla_k{:}\nabla_\omega}_{1} \tag{1}$$

The part indicated by "1" in Equation (1) is the additional term. The expression at the end of the additional term is the inner product tensor. The expansion of the inner product tensor is given in Equation (2).

$$\nabla_k{:}\nabla_\omega = \frac{\partial_k}{\partial_{xj}}\frac{\partial_\omega}{\partial_{xj}} = \frac{\partial_k}{\partial_x}\frac{\partial_\omega}{\partial_x} + \frac{\partial_k}{\partial_y}\frac{\partial_\omega}{\partial_y} + \frac{\partial_k}{\partial_z}\frac{\partial_\omega}{\partial_z} \tag{2}$$

The SST turbulence model was preferred in the solution for the aerodynamic analysis in this study because it aims to overcome the shortcomings of the standard k-ω model, the dependence of k and ω on the free flow values, and can provide effective solutions for flow separations [19–21].

2.4 Prediction methods

In the literature, there are various modeling approaches used in the modeling and estimation of the dynamical system responses [22–24]. While approaches such as regression and multilinear regression are frequently used to model and estimate linear systems, linear approaches do not give effective results in modeling and estimating nonlinear systems. For this reason, artificial intelligence algorithms have recently been successfully used in the modeling of nonlinear systems [25, 26]. In this section, the modeling approaches used in this study are briefly described.

2.4.1 Multilinear regression method

The Multilinear regression model is used in modeling of linear systems; it is used to estimate a dependent variable with more than one independent variable. It is based on optimising the coefficients of the dependent variable to estimate an independent variable, and can be expressed according to Equation (3)

$$y = \beta + w_1x_1 + w_2x_2 + w_3x_3 + \ldots + w_nx_n \tag{3}$$

where y, x_i, and w_i express the independent variable, dependent variable, bias variable and the weight of the independent variable, respectively. Although the multilinear regression model generally gives
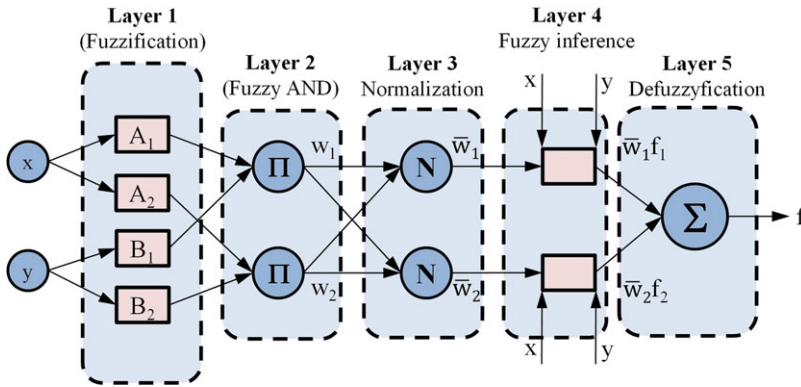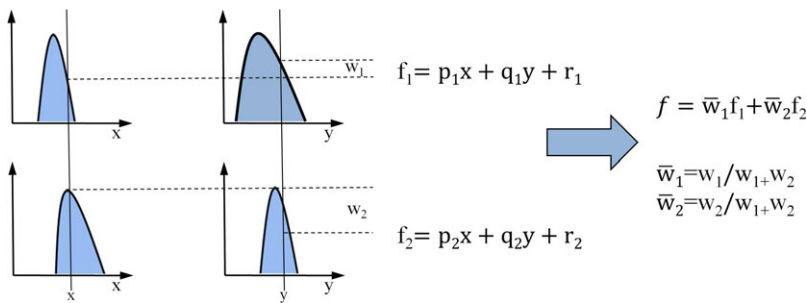
Figure 5. *ANFIS structure [30].*

Figure 6. *The ANFIS premise process [30].*

successful results in modeling linear systems, this is less the case in modeling nonlinear systems. To address this issue, many artificial intelligence-based modeling approaches have been proposed in the literature [27–29].

2.4.2 Adaptive neuro-fuzzy inference systems (ANFIS)
ANFIS, proposed by Jang in 1993, is a modeling approach that combines the parallel computing capabilities of artificial neural networks and the heuristic computing capabilities of fuzzy logic systems. ANFIS can often be trained without specialist knowledge to design a classical fuzzy logic system. An input-output-based dataset is generally needed to apply the ANFIS method. The typical architecture of ANFIS is presented in Figs 5 and 6 [30].

For simplicity, the architecture of ANFIS is presented in Fig. 5 for a two-input one-output system. Figure 6 presents a visual representation of the theoretical model of ANFIS.

Although ANFIS is easier to design than a classical fuzzy logic system, tuning its parameters significantly increases modeling success [31]. Various algorithms have been proposed in the literature to determine optimum parameters. Differing from classical optimisation approaches, various metaheuristic search algorithms have been proposed in the literature [32, 33].

In this section, the genetic algorithm, artificial colony algorithm, and ant colony algorithms used in the training of ANFIS are briefly discussed. A genetic algorithm, inspired by the science of genetics, is a heuristic algorithm for solving complex problems that cannot be answered with classical optimisation techniques [34]. Genetic algorithms are frequently used in optimisation processes and their success has been proven in the literature [35]. Particle swarm optimisation (PSO) is a heuristic algorithm inspired by

Table 3. *Optimisation parameters of the GA, ACO and PSO algorithms*

GA parameters		ACO parameters		PSO parameters	
Parameter	Value	Parameter	Value	Parameter	Value
Maximum iteration	1,000	Maximum iteration	1,000	Maximum iteration	1,000
Size of population	100	Size of population	30	Size of population	40
Crossover percentage	0.7	Intensification factor	0.4	Inertia weight	1
Mutation percentage	0.5	Deviation-distance ratio	1	Inertia weight damping rate	0.99
Gamma	0.2			c1 (Personal learning coefficient)	1
Mutation rate	0.1			c2 (Global learning coefficient)	2
Beta	8				
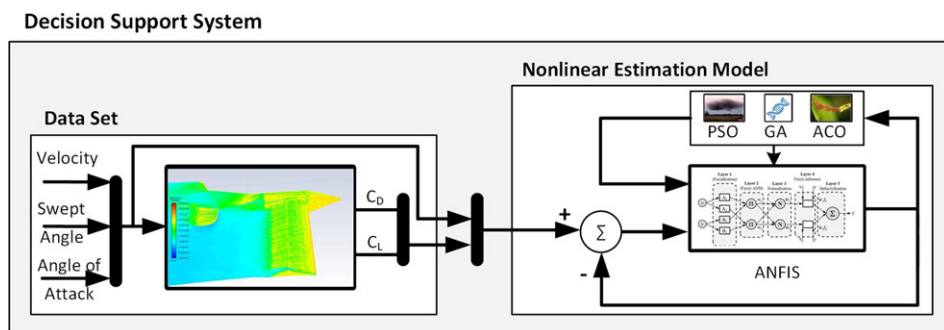
Figure 7. *Schematic diagram of the proposed approach.*

the swarm behaviour of animals when they meet basic needs such as finding food [36]. Ant colony optimization (ACO), a heuristic optimisation algorithm, was introduced in 1991 by Dorigo et al. [37]. Since the algorithm was introduced, various versions have been developed and applied to different optimisation problems [38, 39].

The optimisation parameters are determined by testing traditional functions such as Rastrigin, Ackley, and Goldstein–Price functions. In this study, ACO, Genetic Algorithm (GA) and PSO parameters were chosen by examining the literature [22, 40–43]. Optimisation parameters for metaheuristic algorithms discussed in the study are presented in Table 3.

3.0 Decision support system design

The decision support system consists of two stages, as presented in Fig. 7. In the first stage, the lift and drag coefficients were numerically computed via CFD methods provided by ANSYS. In CFD analysis, 350 datasets, including the independent variables (velocity, swept angle and angle-of-attack) and the dependent variables (drag and lift forces), were created using 5 velocities, 14 swept angles, and 5 angles of attack to cover all possible flight conditions. The accuracy of the numerical results has been confirmed by the experimental results presented in Refs (13, 14). In the second stage, three nonlinear estimation models were created using the PSO, GA and ACO algorithms in the ANFIS structure, where the datasets obtained in the first stage were utilised as training datasets. In addition, a multilinear regression model was also designed to allow for a comparative analysis to investigate the effectiveness of nonlinear models.
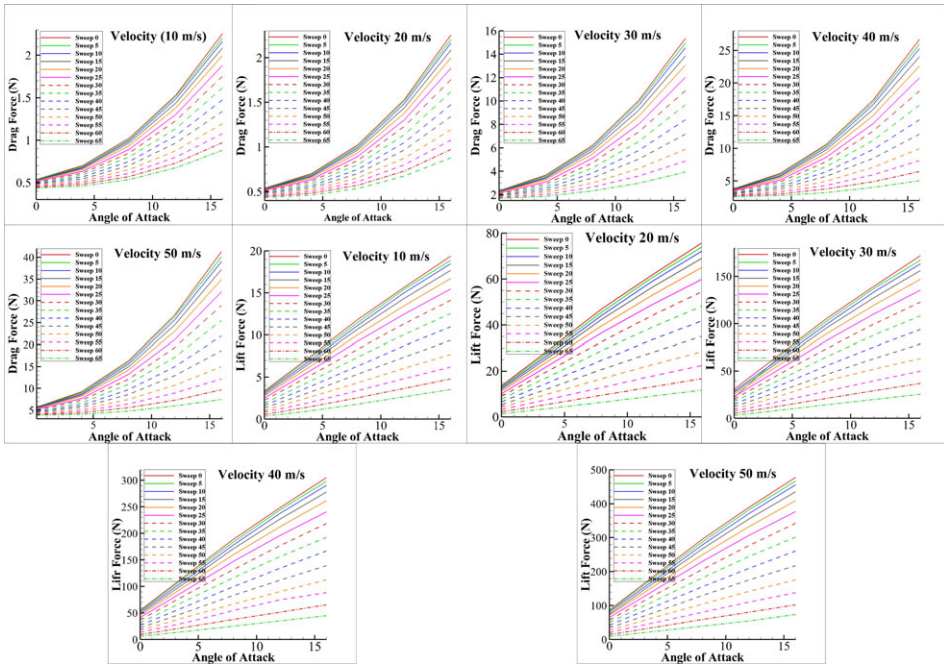
Figure 8. *Variation of aerodynamic force coefficients according to different velocities and swept angles.*

Figure 8 shows that lift force and drag force gradually increase with angle-of-attack at different velocities. Although the lift coefficient tends to decrease with the change in the swept angle, the increase in the swept angle eliminates the possibility of an abrupt stall. Although the increase in the swept angle reduces the total lift force (F) and the lift coefficient, extra lift control is needed for high velocity flight. Drag force (D) also increases with increasing angle-of-attack, but a sudden increase occurs after the stall angle. When the graphs are examined, the increase in the swept angle significantly reduces the variation of the drag force with angle-of-attack. Although the increase in the swept angle causes an increase in the drag coefficient, the use of a variable swept angle will result in a lower drag force at high velocity flight. This means that there will be fuel savings and increased aircraft flight performance as variable swept designs at higher velocities are exposed to reduced levels of drag. Similarly, increasing the swept angle reduces the lift and drag force due to the reduced wing area. However, this reduces the lift force more than the drag force, which has a negative effect on aerodynamic efficiency. The variation of aerodynamic fines (E_{max}) with different velocities is given in Fig. 9.

The Clark-Y aerofoil used in the study was compared with an experimental study in the literature. It was compared with Silvestren's design, with Re = 365,000 and AR = 7.2, and a design with Re = 300,000 and AR = 10 [44]. The results are presented in Fig. 10. When the figure is examined, the aerodynamic analysis shows certain similarities.

In this study, the aerofoil of the variable swept aircraft design is Clark-Y. Fuselage and wings were analysed together to determine aerodynamic parameters. Therefore, when the angle-of-attack increases, the hull's contribution to the carrying force is substantial. The lift and drag forces given in the aerodynamic parameters are for the fuselage and wing form. However, to be able to compare with the literature, the lift and drag coefficients of the plain wing for a velocity of 30m/s were also calculated. The Clark-Y aerofoil achieved its maximum lift coefficient at an approximately 22° angle-of-attack [14].

The 350 datasets obtained from the aerodynamic analysis were used as model input to estimate drag and lift force. First, 250 variations of swept angle, angle-of-attack, and velocity values were selected as independent variables to estimate the drag force. The drag force corresponding to each dataset was defined as the dependent variable. First, a multilinear regression approach analysis, which is one of the
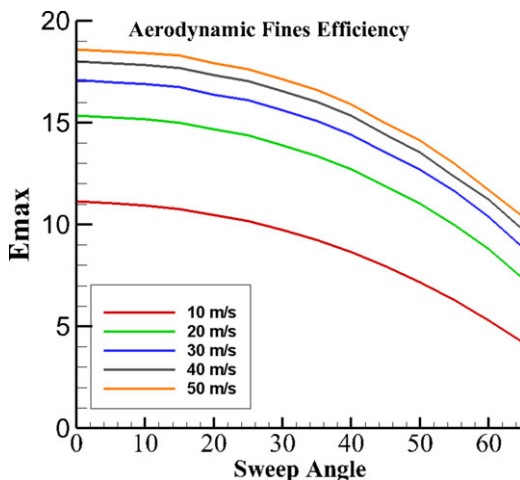
Figure 9. *Variation of aerodynamic fines (E_{max}) according to different velocities.*
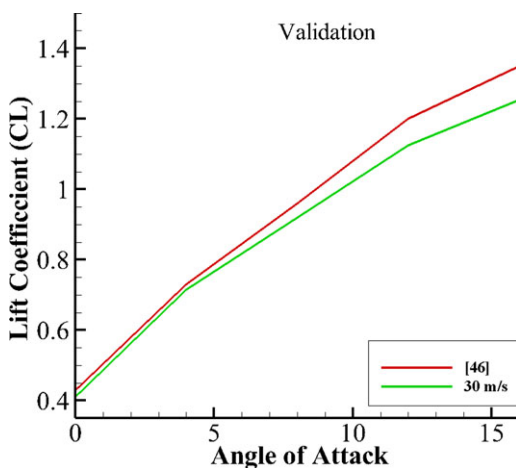

Figure 10. *Comparison of lift coefficient variation with angle-of-attack.*

conventional regression approaches frequently used in the literature, was performed. The multilinear regression equation for drag force is presented in Equation (4).

$$\text{Drag Force} = -4.881 + 0.316v - 0.105\Lambda + 0.608\alpha \qquad (4)$$

To demonstrate the model's success, 100 previously unused datasets were applied to multiple linear regression analysis; model success was evaluated via statistical parameters. In the statistical analysis, the R^2, RMSE, and MAE values for the 250 training sets were respectively calculated as 0.694, 3.85, and 2.794. For 100 test data, the R^2, RMSE, and MAE values were respectively calculated as 0.659, 4.416, and 3.096.

To increase the model success obtained with the multilinear regression approach, ANFIS models, based on metaheuristic algorithms that have been applied in different areas, have been proposed in the literature. Unlike conventional ANFIS structures, the ANFIS training parameters are optimised using the ACO, GA and PSO algorithms. Training and test responses from ACO-, GA- and PSO-based ANFIS trainings are presented in Fig. 11.

Table 4. *Statistical results for drag*

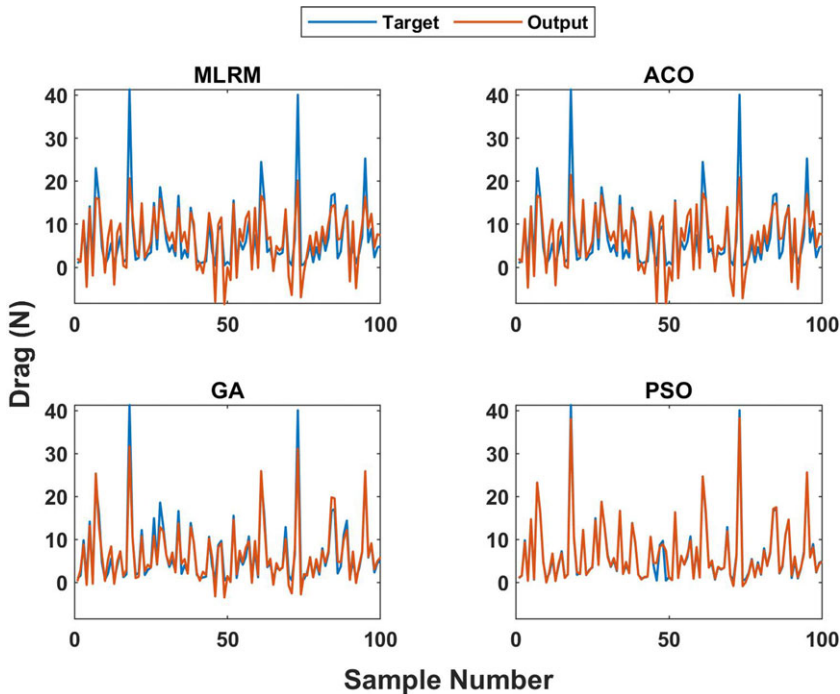|	MLRM		ACO		GA		PSO	
	Train	Test	Train	Test	Train	Test	Train	Test
R^2	0.694	0.659	0.699	0.662	0.957	0.928	0.997	0.983
RMSE	3.85	4.416	3.831	4.426	1.447	2.074	0.34	0.983
MAE	2.794	3.096	2.871	3.165	1.007	1.376	0.26	0.47

Figure 11. *Drag prediction using the MLRM model and the ACO-/GA-/PSO-based ANFIS models.*

While performing metaheuristic-based ANFIS training, 250 different variations of swept angle, angle-of-attack and velocity values were defined as independent variables to estimate drag force. The drag force corresponding to each dataset was defined as the dependent variable. The purpose of using 100 datasets, which were never used in the training process, for testing is to avoid memorisation of the model and to provide a proper learning process. The statistical parameters calculated for the model responses based on metaheuristic algorithms are presented in Table 4. When Table 4 is examined, the PSO-based ANFIS model apparently shows the best performance with an R^2 of 0.983.

Scatter plots are presented in Fig. 12 a, b, c and d that reveal the success of the models obtained within the scope of the study. In the scatter graphs, the *x*-axis defines the model responses, whilst the *y*-axis defines the target to be estimated. In the scatter plot, the linear line expresses the change of target data according to target data. The markers represent the change in the target data according to the model output. For this reason, the model's success is measured according to the linearity of the markers. As can be clearly seen from the scatterplots, the PSO-based ANFIS model predicted the drag force more successfully than all other models.
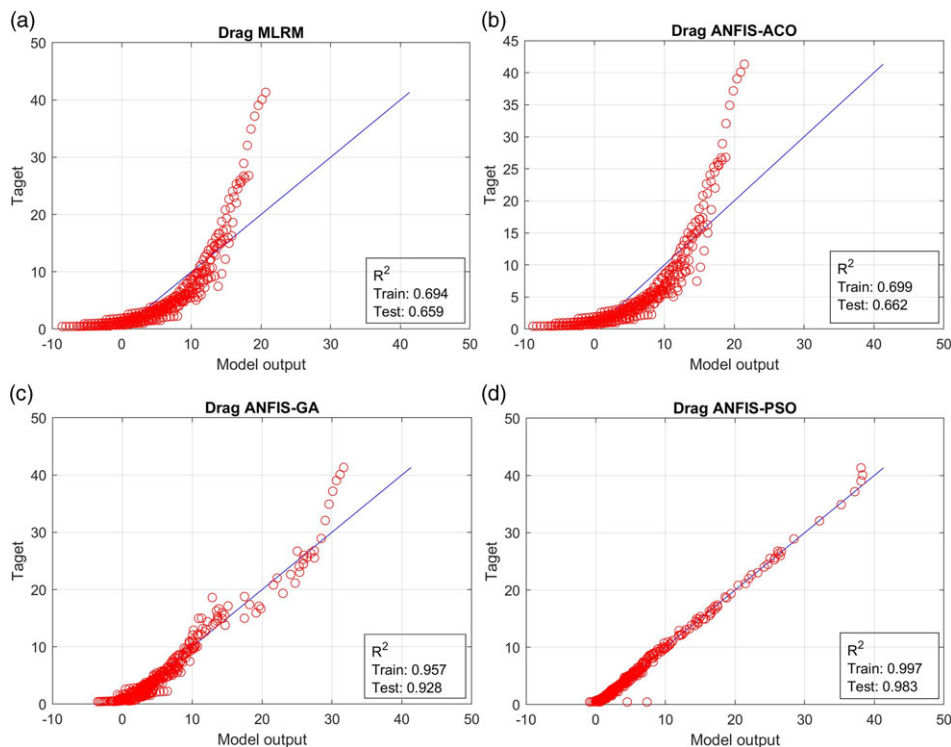
Figure 12. *Scatter graphs for drag predictions (a) MLRM, (b) ACO-based ANFIS, (c) GA-based ANFIS and (d) PSO-based ANFIS.*

In the estimation of the lift force, a process similar to the one followed in the estimation of the drag force was followed. First, 150 of the 180 datasets were used to determine the parameters of the multilinear regression model. The model equation for the lift force is presented in Equation (5).

$$\text{Lift Force} = -54.805 + 4.367v - 1.691\Lambda + 6.999\alpha \tag{5}$$

The success of the multilinear regression model in predicting the lift force was demonstrated by evaluating 100 previously unused datasets with Equation (5). In the statistical analysis, the R^2, RMSE and MAE values for the 250 training datasets were respectively calculated as 0.723, 48.287 and 35.347. For 100 test data, R^2, RMSE and MAE values were respectively calculated as 0.706, 55.364 and 40.937. The results of the multilinear regression model for the training and test data are presented in Fig. 13.

Estimation of lift force was calculated using metaheuristic-based ANFIS models. The model results in which the ANFIS training parameters were optimised with the ACO, GA and PSO algorithms are presented in Fig. 13.

While training the metaheuristic-based ANFIS models in the estimation of lift force, 250 different variations of swept angle, angle-of-attack and velocity values were defined as independent variables, in a similar manner to the training process for the drag force. The lift force corresponding to each data was defined as the dependent variable. One hundred datasets that had never been used in the training process were used for the test. The statistical parameters calculated for ANFIS based on the ACO, GA and PSO models are presented in Table 5. When the table is examined, it is clear that the GA-based ANFIS model has the highest performance with an R^2 of 0.995.

In order to demonstrate the success of the models obtained within the scope of the study, scatter plots of the lift force are presented in Fig. 14 a, b, c and d. When the scatter plots are examined, the results of the PSO-based ANFIS model are clustered on the linear line. This indicates that the PSO-based ANFIS model predicts lift force more successfully than all other models.

Table 5. *Statistical results for lift*

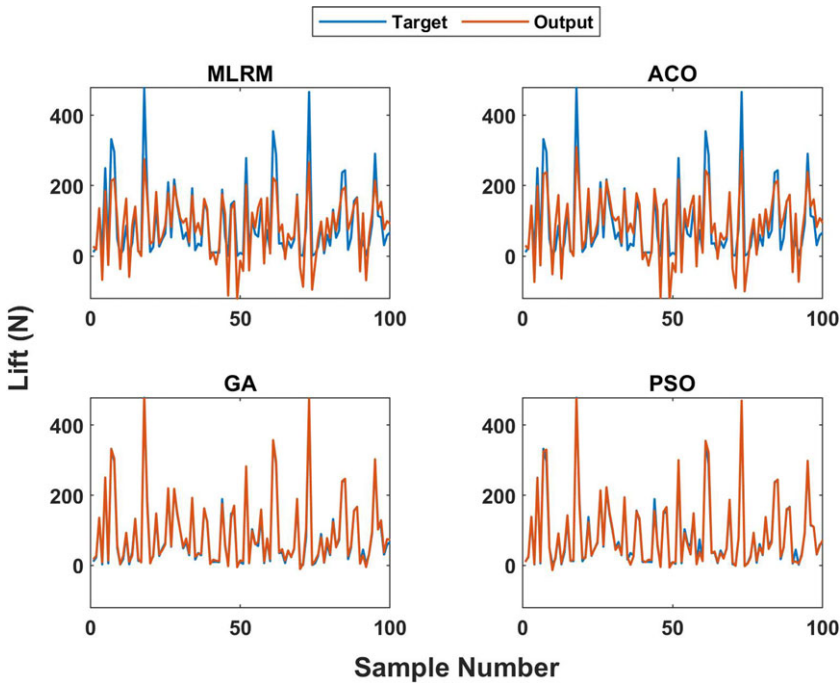|	MLRM		ACO		GA		PSO	
	Train	Test	Train	Test	Train	Test	Train	Test
R^2	0.723	0.706	0.739	0.731	0.989	0.995	0.992	0.991
RMSE	48.287	55.364	47.481	53.372	9.879	7.675	8.388	10.306
MAE	35.347	40.937	36.680	40.998	6.332	6.047	4.184	6.605

Figure 13. *Lift prediction using the MLRM model and the ACO-/GA-/PSO-based ANFIS models.*

4.0 Swept angle estimation approach for minimum lift force

The decision support system enables us to estimate the maximum swept angle producing the minimum lift required for the steady-level flight of the morphing UAV. In addition, it also generates the minimum drag force. The application of the decision support system is presented in Fig. 15.

It is a well-known fact that lower required power leads to higher endurance. The endurance is inversely proportional to the reduction in the required power, and the required power is directly related to the minimum drag force. Thus, the minimum power (maximum endurance) condition occurs when the drag force is at a minimum. Because the morphing mechanism's adjustment of the swept angle of the wing enables a decrease in drag force, endurance can be maximised.

Therefore, the endurance efficiency can be computed as follows:

The drag force coefficient is given by

$$C_D = C_{D_0} + \frac{C_L{}^2}{\pi e AR} \text{ where } L = \frac{1}{2}\rho V^2 S C_L \text{ and } D = \frac{1}{2}\rho V^2 S C_D \tag{6}$$

By using Equation (6), the drag force can be computed as follows:

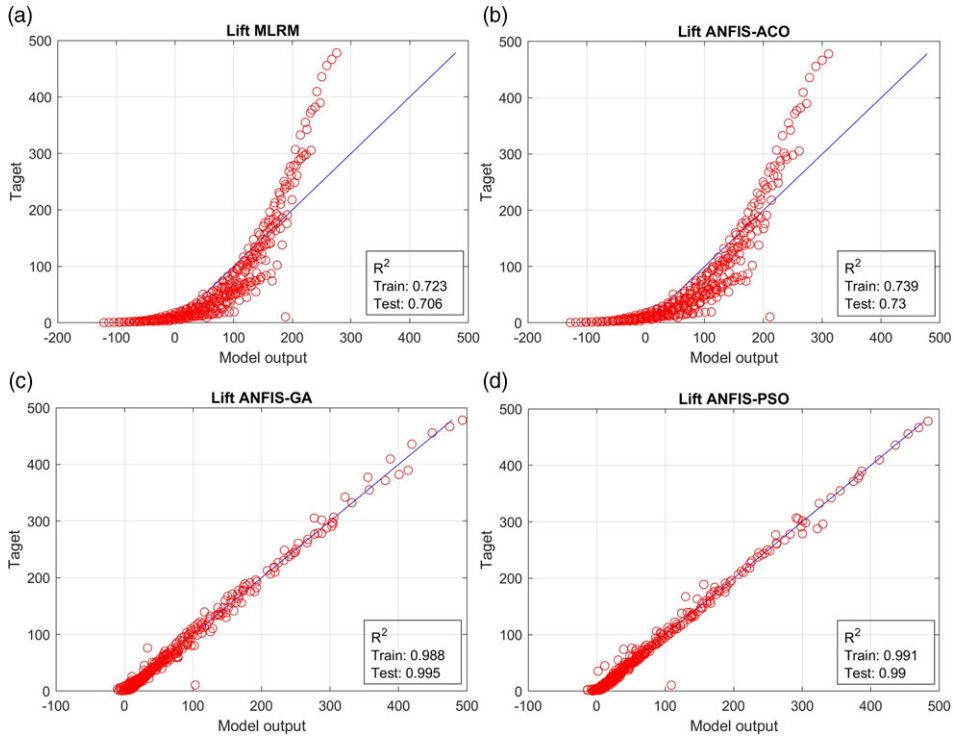$$D = \frac{1}{2}\rho V^2 S C_{D_0} + \frac{W^2}{\frac{1}{2}\rho V^2 S}\left(\frac{1}{\pi e AR}\right) \tag{7}$$

Figure 14. *Scatter graphs for lift predictions (a) MLRM, (b) ACO-based ANFIS, (c) GA-based ANFIS and (d) PSO-based ANFIS.*
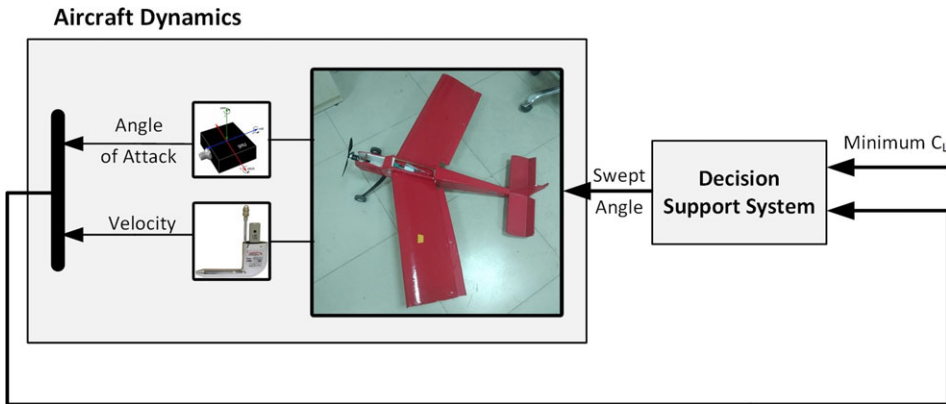
Figure 15. *The application of the decision support system.*

For the steady level flight, the required thrust must be equal to the drag force (Equation (7)), i.e. $T_{req} = D$. Therefore, the required power becomes

$$P_{req} = T_{req}V = DV \tag{8}$$

Finally, substituting Equation (7) into Equation (8) yields:

$$P_{req} = \frac{1}{2}\rho V^3 S C_{D_0} + \frac{W^2}{\frac{1}{2}\rho VS}\left(\frac{1}{\pi eAR}\right) \tag{9}$$

which is used to compute the required power.

Table 6. *Comparison of DSS and CFD results*

Velocity	AoA	Swept angle	Lift (CFD)	Drag (DSS)	Drag (CFD)	Drag (nonmorphing)	% Drag reduction	increase (min)
20.1	6.2	**31.1**	27.68064	2.0939	1.929792	2.475	22.028	3.42
16.3	11.3	**33.9**	22.751	2.0017	2.07289	2.764393	25.014	3.62
29	15.1	**60.8**	30.78043	3.9456	3.71646	14.03676	73.523	5.93
32.7	0.9	**34.9**	26.464	2.1716	2.3891	2.87925	17.023	2.13
26	8.5	**50.6**	30.51615	2.4641	2.35135	3.384475	30.525	3.89
19.3	6.1	**28.7**	24.19389	2.0339	1.834938	2.303845	20.353	3.32
18.2	5.0	**20.6**	23.7407	1.757	1.7344	1.9154	9.449	1.63
16.4	5.9	**20**	27.78287	1.8296	1.79254	1.93488	7.356	1.23
29.2	5.2	**49.1**	29.5387	2.3089	2.3853176	4.032304	40.844	5.13
23.8	3.0	**26**	26.9224	1.7234	1.9094	2.1589	11.556	1.81
27.5	2.7	**49.15**	27,47008	1.5948	1.643963	2.502873	34.316	6.26

In the simulation analysis, two different aircraft configurations are considered. In the first configuration, the swept angle was set to zero, whereas the second configuration was built using a swept wing. To assess the effectiveness of the proposed method, 11 datasets composed of various velocities ranging from 15 to 33m/s and angles of attack ranging from 1° to 12° were randomly selected. The swept angles that produce the optimal lift forces for these selected velocities and angles of attack are estimated using the decision support system introduced in Section 3. The estimated lift and drag forces are then compared with the numerical results obtained from the CFD analyses to determine the accuracy of the estimation approach. In addition, the drag force for the aircraft configuration with non-morphing wings was also computed in a CFD analysis. The percentage reduction in drag force was then computed when a swept wing configuration was utilised. The comparative results are presented in Table 6.

According to the results in Table 4, the lift and drag forces obtained with the estimated swept angle are consistent with those obtained from CDF analysis. The proposed method is able to reduce the drag force significantly for all flight conditions. The maximum reduction is approximately 73%, which is achieved for the flight condition given by a velocity of 29m/s and @ @an angle-of-attack of 15.1°. Moreover, the proposed DSS also improves the endurance of the morphing UAV. When a standard lipo battery is used for the designed, electrically powered UAV, the instantaneously required current can be calculated by considering the drag force. Endurance (min) can be calculated for battery capacity and instantaneous current values. The results show that it can increase endurance by varying between 1.23 and 6.26 min.

5.0 Conclusion

In this study, a UAV with variable swept angles was designed and an aerodynamic analysis was carried out for a range of flight conditions to compare the performance of the designed swept wing UAV with that of the non-swept wing UAV. To cover the majority of the flight envelope, 5 different velocities, 5 different angles of attack, and 14 different swept angle values were considered. The lift force and drag forces were calculated for all possible flight conditions generated using these three different variables in the CFD analysis. The results of the CFD analysis have been verified by experimental studies in the literature. Then, 350 datasets were selected from the CFD analysis to be used in the training and testing processes of the ANFIS structure. The ANFIS models were improved using certain metaheuristic algorithms, i.e., ABC, GA and PSO. The estimation accuracies of the ANFIS models were compared with that of the multilinear regression model, which is a linear modeling approach. From the estimated results, it can be revealed that PSO-based ANFIS model provides higher accuracy in terms of estimating the lift and drag forces than the other models considered for a prescribed velocity, angle-of-attack and swept angle. Therefore, this model was selected to estimate the swept angle required to maintain the minimum lift

force in steady-level flight for a constant velocity and angle-of-attack. The lift and drag forces of the simulation and CFD analysis were compared to investigate whether the estimated swept angle would be sufficient to produce the minimum required lift force. Another comparison was then made to demonstrate how effective the swept configuration would be in terms of reducing the drag force and increasing the endurance. The proposed method can achieve an average reduction of 26% in drag force and an average increase of 3.5 min endurance.

References

[1] Mariga, L., Tiburcio, I.S., Martins, C.A., Prado, A.A. and Nascimento, C. Measuring battery discharge characteristics for accurate UAV endurance estimation, *Aeronaut. J.*, 2020, **124**, (1277), pp 1099–1113.

[2] Li, N., Liu, X., Yu, B., Li, L., Xu, J. and Tan, Q. Study on the environmental adaptability of lithium-ion battery powered UAV under extreme temperature conditions, *Energy*, 2021, **219**, p 119481.

[3] Shao, P., Wu, J., Wu, C. and Ma, S. Model and robust gain-scheduled PID control of a bio-inspired morphing UAV based on LPV method, *Asian J. Control*, 2019, **21**, (4), pp 1681–1705.

[4] Anderson, J.D. and Bowden, M.L. *Introduction to Flight* (Vol. 582), McGraw-Hill Higher Education, 2005, New York.

[5] Li, D., Zhao, S., Da Ronch, A., Xiang, J., Drofelnik, J., Li, Y., Zhang, L., Wu, Y., Kintscher, M., Monner, H.P., Rudenko, A., Guo, S., Yin, W., Kirn, J., Storm, S. and De Breuker, R. A review of modelling and analysis of morphing wings, *Prog. Aerospace Sci.*, 2018, **100**, pp 46–62.

[6] Weaver-Rosen, J.M., Leal, P.B., Hartl, D.J. and Malak, R.J. Parametric optimization for morphing structures design: application to morphing wings adapting to changing flight conditions, *Struct. Multidiscip. Optim.*, 2020, **62**, (6), pp 2995–3007.

[7] Elelwi, M., Kuitche, M.A., Botez, R.M. and Dao, T.M. Comparison and analyses of a variable span-morphing of the tapered wing with a varying sweep angle, *Aeronaut. J.*, 2020, **124**, (1278), pp 1146–1169.

[8] Kundu, A.K. *Aircraft Design* (Vol. 27), Cambridge University Press, 2010, New York, USA.

[9] Yan, B., Dai, P., Liu, R., Xing, M. and Liu, S. Adaptive super-twisting sliding mode control of variable swept morphing aircraft, *Aerospace Sci. Technol.*, 2019, **92**, pp 198–210.

[10] Xu, W., Li, Y., Lv, M. and Pei, B. Modeling and switching adaptive control for nonlinear morphing aircraft considering actuator dynamics, *Aerospace Sci. Technol.*, 2022, **122**, p 107349.

[11] Dai, P., Yan, B., Huang, W., Zhen, Y., Wang, M. and Liu, S. Design and aerodynamic performance analysis of a variable-swept-wing morphing waverider, *Aerospace Sci. Technol.*, 2020, **98**, p 105703.

[12] Roy, A.G. and Peyada, N.K. Aircraft parameter estimation using hybrid neuro fuzzy and artificial bee colony optimization (HNFABC) algorithm, *Aerospace Sci. Technol.*, 2017, **71**, pp 772–782.

[13] Homa, D., Wróblewski, W., Majkut, M. and Strozik, M. Experimental and numerical investigation of cavitation on Clark Y foil, Journal of Physics: Conference Series (Vol. 1101, No. 1). IOP Publishing, 2018, p 012008.

[14] Kheir-aldeen, M. and Hamid, A. Experimental study to the effect of gurney flap on the Clark Y-14 airfoil wing model, *Int. J. Innovation Sci. Res.*, 2014, **9**, (1), pp 120–32.

[15] Douvi, C.E., Tsavalos, I.A. and Margaris, P.D. Evaluation of the turbulence models for the simulation of the flow over a National Advisory Committee for Aeronautics (NACA) 0012 airfoil, *J. Mech. Eng. Res.*, 2012, **4**, (3), pp 100–111.

[16] Wilcox, D.C. Simulation of transition with a two-equation turbulence model, *AIAA J.*, 1994, **32**, (2), pp 247–255.

[17] Menter, F.R., Langtry, R.B., Likki, S.R., Suzen, Y.B., Huang, P.G. and Völker, S. A correlation-based transition model using local variables—part I: model formulation, *J. Turbomach.*, 2006, **128**, (3), pp 413–422.

[18] Langtry, R. and Menter, F. Transition modeling for general CFD applications in aeronautics, 43rd AIAA Aerospace Sciences Meeting and Exhibit, 2005, p 522.

[19] Menter, F.R. *Improved two-equation k-omega turbulence models for aerodynamic flows* (No. A-92183), 1992.

[20] Menter, F. Zonal two equation kw turbulence models for aerodynamic flows, 23rd Fluid Dynamics, Plasmadynamics, and Lasers Conference, 1993, p 2906.

[21] Menter, F.R. Two-equation eddy-viscosity turbulence models for engineering applications, *AIAA J.*, 1994, **32**, (8), pp 1598–1605.

[22] Sevim, U.K., Bilgic, H.H., Cansiz, O.F., Ozturk, M. and Atis, C.D. Compressive strength prediction models for cementitious composites with fly ash using machine learning techniques, *Constr. Build. Mater.*, 2021, **271**, p 121584.

[23] Suresh, S., Omkar, S.N., Mani, V. and Prakash, T.G. Lift coefficient prediction at high angle of attack using recurrent neural network, *Aerospace Sci. Technol.*, 2003, **7**, (8), pp 595–602.

[24] Morgado, J., Vizinho, R., Silvestre, M.A.R. and Páscoa, J.C. XFOIL vs CFD performance predictions for high lift low Reynolds number airfoils, *Aerospace Sci. Technol.*, 2016, **52**, pp 207–214.

[25] Oktay, T., Arik, S., Turkmen, I., Uzun, M. and Celik, H. Neural network based redesign of morphing UAV for simultaneous improvement of roll stability and maximum lift/drag ratio, *Aircraft Eng. Aerospace Technol.*, 2018, **90**, (8), pp 1203–1212.

[26] Bagis, A. and Konar, M. Comparison of Sugeno and Mamdani fuzzy models optimized by artificial bee colony algorithm for nonlinear system modelling, *Trans. Inst. Meas. Control*, 2016, **38**, (5), pp 579–592.

[27] Bilgic, H.H., Guvenc, M.A., Çakır, M. and Mistikoglu, S. A study on prediction of surface roughness and cutting tool temperature after turning for s235jr steel, *Konya Mühendislik Bilimleri Dergisi*, 2019, **7**, pp 966–974.

[28] Bilgiç, H.H. and Mert, İ. Comparison of different techniques for estimation of incoming longwave radiation, *Int. J. Environ. Sci. Technol.*, 2021, **18,** (3), pp 601–618.

[29] Mert, İ., Bilgic, H.H., Yağlı, H. and Koç, Y. Deep neural network approach to estimation of power production for an organic Rankine cycle system, *J. Braz. Soc. Mech. Sci. Eng.*, 2020, **42,** (12), pp 1–16.

[30] Jang, J.S. ANFIS: adaptive-network-based fuzzy inference system, *IEEE Trans. Syst. Man Cybern.*, 1993, **23,** (3), pp 665–685.

[31] Isermann, R. On fuzzy logic applications for automatic control, supervision, and fault diagnosis, *IEEE Trans. Syst. Man Cybern.-Part A Syst. Hum.*, 1998, **28,** (2), pp 221–235.

[32] Shehabeldeen, T.A., Abd Elaziz, M., Elsheikh, A.H. and Zhou, J. Modeling of friction stir welding process using adaptive neuro-fuzzy inference system integrated with harris hawks optimizer, *J. Mater. Res. Technol.*, 2019, **8,** (6), pp 5882–5892.

[33] Han, Z., Chen, M., Shao, S. and Wu, Q. Improved artificial bee colony algorithm-based path planning of unmanned autonomous helicopter using multi-strategy evolutionary learning, *Aerospace Sci. Technol.*, 2022, **122**, p 107374.

[34] Holland John, H. *Adaptation in Natural and Artificial Systems*, University of Michigan Press, 1975, Ann Arbor.

[35] Mirjalili, S. Genetic algorithm, in *Evolutionary Algorithms and Neural Networks*, Springer, 2019, Cham, pp 43–55.

[36] Eberhart, R. and Kennedy, J. A new optimizer using particle swarm theory, MHS'95. *Proceedings of the Sixth International Symposium on Micro Machine and Human Science*, IEEE, 1995, pp 39–43.

[37] Dorigo, M., Maniezzo, V. and Colorni, A. The ant system: An autocatalytic optimizing process, 1991.

[38] Song, M.A.O. and Zhao, C.L. Unequal clustering algorithm for WSN based on fuzzy logic and improved ACO, *J. China Univ. Posts Telecommun.*, 2011, **18,** (6), pp 89–97.

[39] Chen, Y., Bai, G., Zhan, Y., Hu, X. and Liu, J. Path planning and obstacle avoiding of the USV based on improved ACO-APF hybrid algorithm with adaptive early-warning, *IEEE Access*, 2021, **9**, pp 40728–40742.

[40] Rao, R.V., Savsani, V.J. and Vakharia, D.P. Teaching–learning-based optimization: an optimization method for continuous non-linear large scale problems, *Inf. Sci.*, 2012, **183,** (1), pp 1–15.

[41] Nagaraj, B. and Murugananth, N. A comparative study of PID controller tuning using GA, EP, PSO and ACO, 2010 *International Conference On Communication Control And Computing Technologies*, IEEE, 2010, pp 305–313.

[42] Adrian, A.M., Utamima, A. and Wang, K.J. A comparative study of GA, PSO and ACO for solving construction site layout optimization, *KSCE J. Civil Eng.*, 2015, **19**, pp 520–527.

[43] Tam, J.H., Ong, Z.C., Ismail, Z., Ang, B.C. and Khoo, S.Y. A new hybrid GA− ACO− PSO algorithm for solving various engineering design problems, *Int. J. Comput. Math.*, 2019, **96,** (5), pp 883–919.

[44] Silverstein, A. *Scale effect on Clark Y airfoil characteristics from NACA full-scale wind-tunnel tests* (No. NACA-TR-502), 1935.